Nanochem Res 5(2): 154-167, Summer and Autumn 2020

RESEARCH PAPER

Simple manufacturing and metal type-dependent properties of $M_3(OH)_2V_2O_{7\cdot n}H_2O$ (M; Co, Ni, Cu, Zn) nanostructures

Berna Bülbül [1], Seda Beyaz [1,*], Mustafa Akyol [2], Ahmet Ekicibil[3]

[1] Department of Chemistry, Science-Literature Faculty, Balikesir University, Balikesir, Turkey.

[2] Department of Materials Engineering, Adana Science and Technology University, Adana, Turkey.

[3] Department of Physics, Science-Literature Faculty, Çukurova University, Adana, Turkey.

ARTICLE INFO

Article History:
Received 03 August 2020
Accepted 06 October 2020
Published 15 October 2020

Keywords:
Nanovanadates
Zn
Co
Ni
Cu

ABSTRACT

$M_3(OH)_2V_2O_7{\cdot}nH_2O$ (M : Co, Ni, Cu, Zn) nanostructures were synthesized by a simple and economic chemical precipitation route. For Co and Ni compounds, very small (~9 nm), irregularly shaped and poor crystalline nanoparticles occurred, probably due to high tendency for complexing with ammonia molecules releasing from ammonium metavanadate. However, more crystalline Co compounds could be synthesized in high reactant concentrations, but not for Ni. Zn and Cu compounds are well crystallized in the hexagonal and monoclinic unit cell, respectively. Their shapes were nanoflake or nanoplate and their thickness were about 20 nm and 25 nm, respectively. Both have an average diameter of less than 500 nm. The chemical formulas determined were $Co_3V_2O_7(OH)_2{\cdot}2.8H_2O$, $Ni_3V_2O_7(OH)_2{\cdot}5.6H_2O$, $Cu_3V_2O_7(OH)_2{\cdot}2H_2O$ and $Zn_3V_2O_7(OH)_2{\cdot}2.8H_2O$. The band gaps of samples were found in the range from 3.22 to 4.34 eV. Magnetic measurements show that all Co samples have a magnetic transition from ferromagnetic (FM) to paramagnetic (PM) around 300 K, on the ground that samples with FM characteristics and coupling at 5 K temperature turn into PM samples at room temperature. These results are important for large-scale synthesis of nanovanadate structures.

How to cite this article
Bülbül B., Beyaz S., Akyol M., Ekicibil A. Simple manufacturing and metal type-dependent properties of $M_3(OH)_2V2O_{7\cdot n}H_2O$ (M; Co, Ni, Cu, Zn) nanostructures. Nanochem Res, 2020; 5(2):154-167. DOI: 10.22036/ncr.2020.02.006

INTRODUCTION

In recent years, many researchers have shown interest in vanadium-based metal oxides for their electronic technological applications such as lithium rechargeable battery [1, 2] due to their layered nature, excellent kinetics, and heterogeneous catalytic feature [3, 4]. Besides, many vanadates contain crystal water which exists as OH groups on the external and internal surfaces. This enhances the reversible capacity, because the extra oxygen in the crystal water facilitates the formation of "Li–O" type binding in the low voltage reduction process [5, 6]. The most important advantage of these vanadates is their lower formation energy compared to other oxide compounds, thus rapidly opening up to synthesis with colloidal chemistry, while at the same time preventing agglomeration of nanoparticles at higher reaction temperatures. The methods used to prepare these materials are mostly the hydrothermal [1, 2, 4] based techniques requiring high temperature and pressure environment, though the amount of product obtained with these techniques is quite small.

Despite the great advantages of precipitation method including simplicity, high reaction rates, and cost-effective synthetic procedure for preparing of vanadate nanostructures, not many works have been performed using this technique [3, 7]. Recently, several novel facile methods have been

* Corresponding Author Email: *sedacan@balikesir.edu.tr*

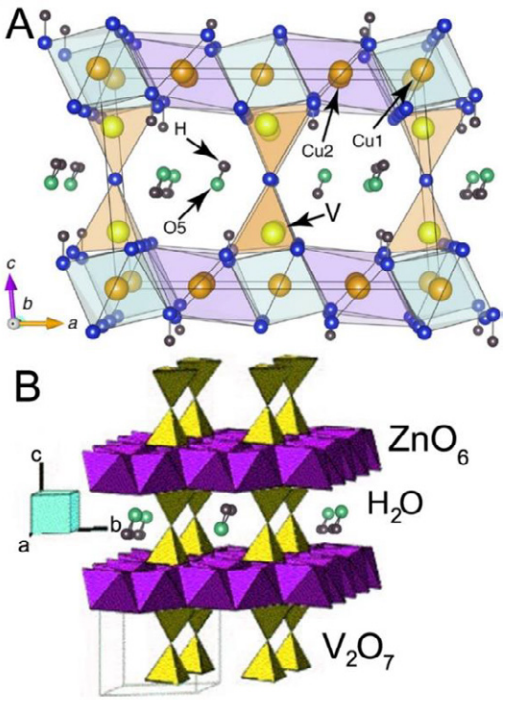

Fig. 1. Structures of $Cu_3(OH)_2V_2O_7.nH_2O$ (A) and $Zn_3(OH)_2V_2O_7.nH_2O$ (B)

proposed to synthesize transition metal vanadates under an ambient environment [8, 9].

We have recently explored a new approach for preparing nanovanadate compounds at room temperature [10, 11]. This approach is based on the increase of solubility of NH_4VO_3 in water by adding NaOH. The general equations for the synthesis are as follow:

$$NH_4VO_3 + 3NaOH \rightarrow Na_3VO_4 + NH_3 + 2H_2O \quad (1)$$

$$Na_3VO_4 + M(NO_3)_3.nH_2O \rightarrow MVO_4 + 3NaNO_3 + nH_2O \quad (2.1)$$

or

$$2Na_3VO_4 + 3M(NO_3)_2.nH_2O \rightarrow M_3(OH)_2V_2O_7 + 6NaNO_3 + (3n-1)H_2O \quad (2.2)$$

Herein, we have selected cobalt, nickel, copper and zinc as metal owing to their wide range of applications, thus $M_3(OH)_2V_2O_7{\cdot}nH_2O$ (M; Co, Ni, Cu, Zn) compounds were synthesized according to Equation 2.2 since their ion valences are 2+.

Volborthite ($Cu_3(OH)_2V_2O_7.2H_2O$) has an interesting crystalline structure that is of porous framework [12] as shown in Fig. 1, so it is a potential candidate for many applications in different areas. In addition, as a metastable phase, it can be used as an active starting material for preparing other new advanced mixed oxides based on vanadium and copper. The $Cu_3(OH)_2V_2O_7.2H_2O$ nanoparticles were successfully synthesized via hydrothermal method [1]. Their magnetic and electrochemical properties as a positive electrode of lithium ion battery were studied by Ni et al [1, 13]. Zhang et al. [7, 14] also performed the cyclic voltammograms of the electrode materials made from the as-prepared $Cu_3(OH)_2V_2O_7.2H_2O$ and reported that nanowires, nanoflakes, and nanoparticles exhibited high discharge capacities and ideal shaped discharge curves. Melghit et al. [15] prepared a pure copper pyrovanadate by mixing copper monoxide Cu_2O with a solution of vanadium oxide xerogel, $V_2O_5.2H_2O$, for a long time. Besides, different copper-organic complexes such as $[Cu(en)_2]SO_4$, [Cu (TETA)] SO_4 were used as Cu precursor in a precipitation method and then the synthesized copper pyrovanadate was added to the polymer solutions (Poly vinyl alcohol, poly styrene) to investigate its influence on the flame retardancy, by Arani et al. [16].

Martyite or zinc pyrovanadate, ($Zn_3(OH)_2V_2O_7{\cdot}2H_2O$) was first prepared under

hydrothermal conditions at 438 K in 1997 [17] . It consists of alternated Zn–O layer and V–O layer with channels in V–O layer [18]. Water molecules fill the large cavities; they are attached by hydrogen bonds to hydroxyl groups present in the structure (Fig. 1). It has the potential to be used as a negative material for the lithium ion battery due to the channel structure in the V-O layer [2]. In addition, zinc pyrovanadate exhibits efficient UV-light-driven photocatalytic activity for the degradation of methylene blue [3, 4, 19, 20].

Recently, well-crystallized $Zn_3(OH)_2V_2O_7.nH_2O$ nanosheets were successfully synthesized by Ni et. al and their optical, magnetic and photoluminescence properties were reported in a series of papers [2, 21-23]. However, studies on nano- and micro-scale $Zn_3(OH)_2V_2O_7.nH_2O$ particles are limited [24, 25].

To the best of our knowledge, experimental report about a simple and rapid chemical precipitation synthesis of $Cu_3(OH)_2V_2O_7.nH_2O$ and $Zn_3(OH)_2V_2O_7{\cdot}nH_2O$ without surfactant or template has been rare by now. Moreover there is only one report [26] for hydrothermal synthesis of $Co_3(OH)_2V_2O_7.nH_2O$ and no report available for $Ni_3(OH)_2V_2O_7.nH_2O$.

In this study, $M_3(OH)_2V_2O_7{\cdot}nH_2O$ (M : Co, Ni, Cu, Zn) nanostructures were synthesized by a novel simple and economic precipitation route which will offer great opportunities for the scale-up preparation of novel type metal vanadate nanostructures. In addition to examining the effect of the metal type in the study, the reactant concentration effect on the structural properties of Co compounds was investigated. Remarkable changes were observed in the crystallinity, particle shape and size of samples with changing metal type. Moreover, the crystallinity of Co samples was improved by increasing the reactant concentration.

EXPERIMENTAL

Materials

All the chemicals were of analytical grade and used as received without further purification. Cobalt nitrate ($Co(NO_3)_2.6H_2O$),nickel nitrate ($Ni(NO_3)_2.6H_2O$), copper nitrate ($Cu(NO_3)_2.3H_2O$), zinc nitrate ($Zn(NO_3)_2.4H_2O$), sodium hydroxide (NaOH) and ammonium metavanadate (NH_4VO_3) were purchased from Merck.

Experimental Procedure

In a typical synthesis, 30 mmol NaOH and 10 mmol NH_4VO_3 were added to 20 ml of water and the solution was mixed for 10 min to prepare Na_3VO_4 aqueous solution. The metal solution was also prepared in 20 ml water using 15 mmol of metal nitrate. The solutions were mixed together suddenly in a reaction vessel at 2000 rpm for 30 minutes. Finally, the precipitate was formed at room temperature. After the samples were filtered, they were washed with distilled water for five times and ethanol for one times to remove the impurities completely and then dried at 70 °C for one day. The pH values of the precipitate solutions were measured at around 8.28 for all metals. No pH adjustment was made during the reaction. To increase pH, the initial concentration of NaOH was increased and pH was measured after the reaction was completed.

To investigate the concentration effect in Co samples, while the OH/VO_4/Co ratio was kept constant at 6/2/3, the ionic quantities were increased from 30/10/15 (mmol) to 100/33,33/50 (mmol). Thus, eight samples with different concentrations were synthesized and labeled as Co1 (30/10/15 (mmol)), Co2 (40/13.33/20 (mmol)), Co3 (50/16.67/25 (mmol)), Co4 (60/20/30 (mmol)), Co5 (70/23.33/35 (mmol)), Co6 (80/26.67/40 (mmol)), Co7 (90/30/45 (mmol)), and Co8 (100/33.33/50 (mmol)).

Characterization

The crystallinity and phase studies were carried out using Rigaku Rint 2200 X-ray diffraction (XRD) analyzer with Cu Ka radiation (1.54059 Å) at 30 mA and 40 kV. The Fourier transform infrared spectroscopy (FT-IR) spectra were recorded using Perkin Elmer 65 model FT-IR spectrometer in the range of 4000–600 cm^{-1}. High resolution transmission electron microscopy (HRTEM) investigations were performed on JEOL-2100 HRTEM operating at 200 kV (LaB_6 filament). Images were taken by Gatan Model 794 Slow Scan CCD Camera and also by Gatan Model 833 Orius SC200D CCD camera. Carbon support film coated copper TEM grids (Electron Microscopy Sciences, CF200-Cu, 200 mesh) were used. Additionally, powder samples were coated with 3 nm Au/Pd and visualized under high vacuum with a FEI Quanta 200 FEG scanning electron microscope (SEM) equipped with ETD detector. Thermo-gravimetric analysis (TGA) was carried out using powder samples (~10mg) with a heating rate of 10 °C/min in air atmosphere up to 600 °C using a Perkin-Elmer TG-DTA analyzer. UV-visible diffuse reflectance measurements

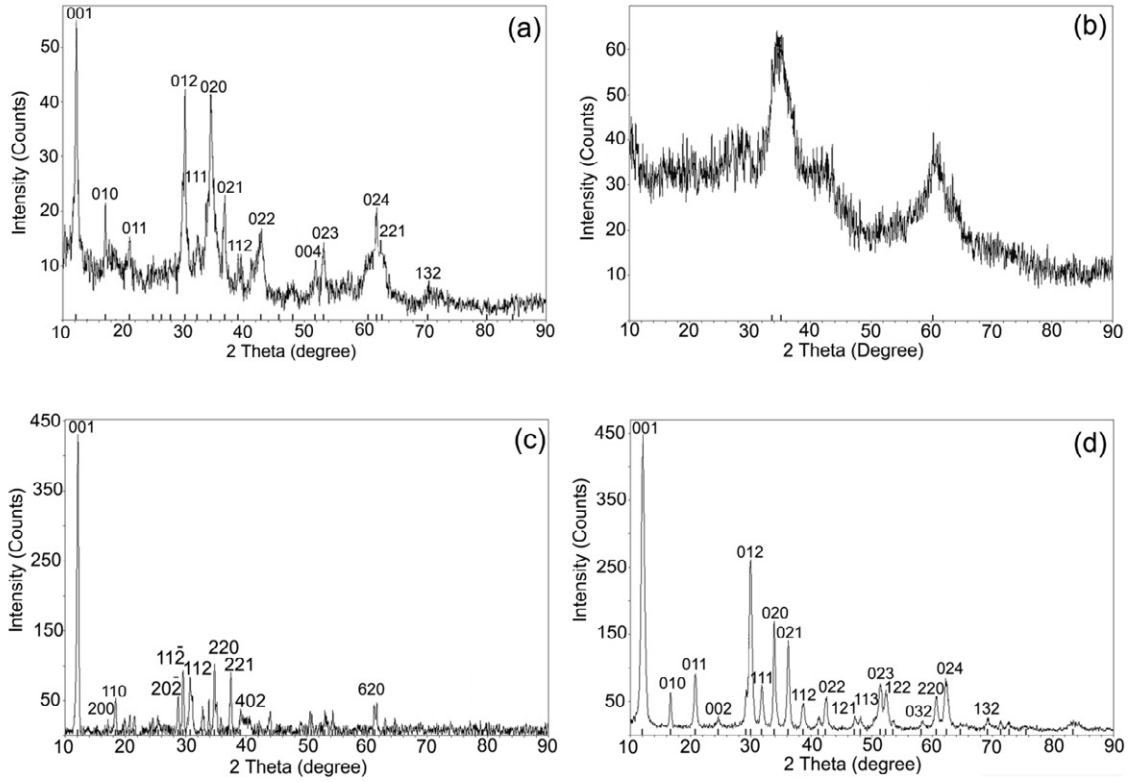

Fig. 2. X ray diffraction patterns of the Co(a), Ni (b),Cu (c) and Zn (d) compounds

were performed by T80 UV/Vis spectrometer (PG Instruments). Elemental analysis was performed by Rikagu ZSX Premius model X-ray fluorescence (XRF). Magnetizations of samples were measured by using a Vibrating Sample Magnetometer (VSM) in Physical Property Measurement System (PPMS, Quantum Design).

Table 1. The complex formation constants of metal ions with ammonia at 25 °C

Amine complex	K_f
$Ni(NH_3)_6^{2+}$	2.0×10^8
$Co(NH_3)_6^{2+}$	5.0×10^4
$Cu(NH_3)_4^{2+}$	1.1×10^{13}
$Zn(NH_3)_4^{2+}$	7.8×10^8

RESULTS AND DISCUSSION

Effect of metal type

$M_3(OH)_2V_2O_7{\cdot}nH_2O$ nanostructures were successfully synthesized using Co, Ni, Cu, Zn transition metals. As can be seen in XRD graphics of Fig. 2, the Cu and Zn compounds are more crystalline than the ones of Co and Ni. Moreover Ni compound has a completely amorphous phase.

As pointed at Table 1, these transition metals have a strong tendency to complex with the NH_3 molecules released in the reaction, shown in Equation 1. Such complexes may prevent vanadate ion collapse or may interfere with nuclei growth by cage effects, thus affecting the crystallinity of the samples. Comparing the tendency for complex formation of ions, Ni and Co are much more willing than Zn and Cu, because they generate a coordination sphere with six ammonia ligands. When a further comparison is made, considering the constants in Table 1, the most desirable ion is nickel [$Ni(NH_3)_6$,K_f : 2x10 ^{8}] and the most reluctant ion is zinc [$Zn(NH_3)_4^{2+}$,K_f: 7.8x10^8], which is compatible with the order of crystallinity of the products: Zn> Cu> Co> Ni.

Volborthite, $Cu_3V_2O_7(OH)_2{\cdot}nH_2O$, adopts monoclinic symmetry due to the significant Jahn–Teller distortion of one of the two symmetrically non-equivalent CuO_6 octahedral. In Fig. 2(c), all the diffraction peaks can be readily indexed to the pure phase of $Cu_3V_2O_7(OH)_2{\cdot}nH_2O$ with the mono-

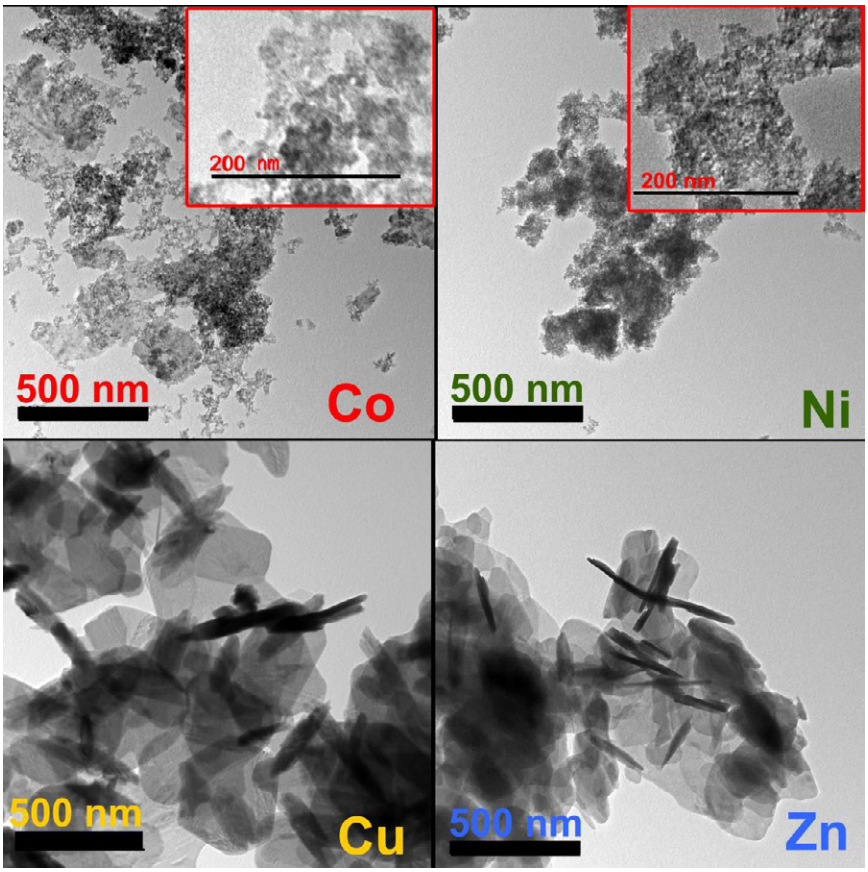

Fig. 3. HRTEM images of Co, Ni, Cu and Zn samples.

clinic structure [JCPDS-ICDD Card No. 80-1170]. Strong and sharp peeks suggest that the as-synthesized products are well crystallized.

The XRD pattern of the as-prepared $Zn_3(OH)_2V_2O_7{\cdot}nH_2O$ product is shown in Fig. 2(d). All diffraction peaks are indexed in hexagonal unit cell similar to the reported unit cell for zinc pyrovanadate (JCPDS card No. 50-0570) [2, 3, 21-23].

The sizes and morphologies of the products were characterized by HRTEM and SEM. Fig. 3 shows the HRTEM images of the products in a typical procedure. When Co and Ni were used in the synthesis of the products, very small (~9 nm) and irregularly shaped nanoparticles were obtained. In a previous study, $Co_3V_2O_7(OH)_2{\cdot}nH_2O$ nanosheets with larger sizes (200 nm to 2 μm) were synthesized by a hydrothermal method but again with irregular shapes [26]. Unfortunately, for nickel, we did not find a study in the literature for comparison . As mentioned earlier, the reason for the small size may be the high complexing effect of the ammonium ions with Ni and Co and as a result, poor crystallization. Another reason might be due to a higher coordination number that provide a better cage effect.

From Fig. 3 and Fig. 4, we can see that the shapes of $Cu_3V_2O_7(OH)_2{\cdot}nH_2O$ and $Zn_3V_2O_7(OH)_2{\cdot}nH_2O$ are nanoflake or nanoplate in accordance to the literature [14]. Fig. 4 (b, d) is a low magnification that exhibits a large quantity of nanoplates for Cu and Zn compounds. While the thickness of $Cu_3V_2O_7(OH)_2{\cdot}nH_2O$ nanoplates is about 25 nm, the thickness of $Zn_3V_2O_7(OH)_2{\cdot}nH_2O$ nanoplates is less, about 20 nm. Both have an average diameter of less than 500 nm. High and low magnification SEM images of $Zn_3V_2O_7(OH)_2{\cdot}nH_2O$ in Fig. 4 (e, f) clearly reveal 3D structure of nanoplates and their tendency to stick to each other (aggregation).

For further clarification of the composition of the samples, their thermal behaviors are investigated by means of TG measurement in air atmosphere at a heating rate of 10 K min^{-1}. The TGA curves at Fig. 5 exhibit the weight losses between 25 °C and 600 °C due to the elimination of water molecules

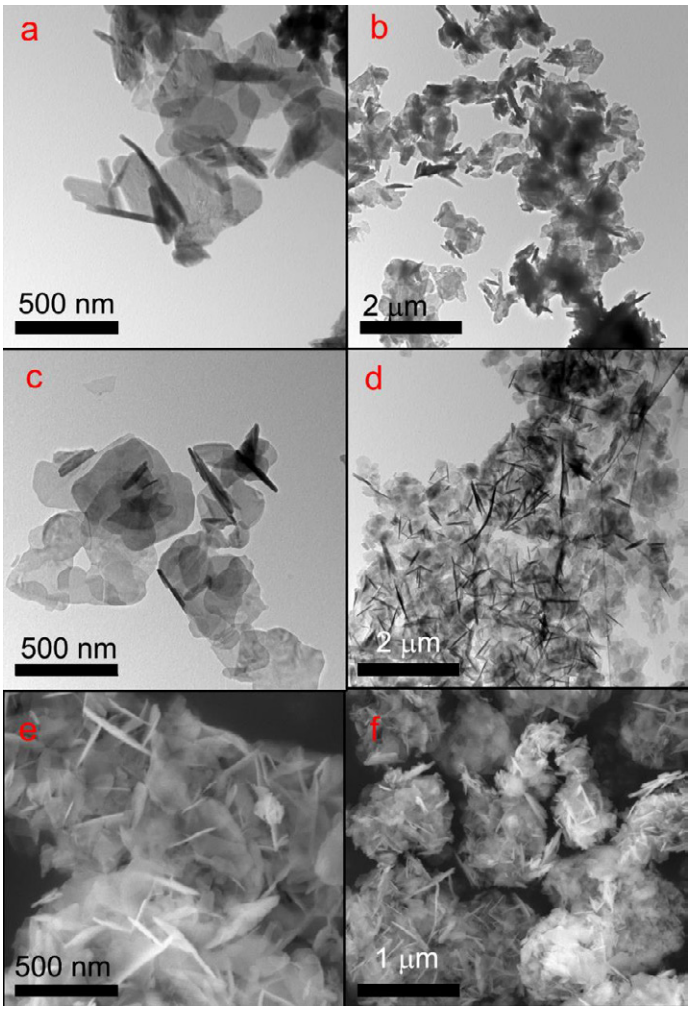

Fig. 4. HRTEM images of (a,b) $Cu_3V_2O_7(OH)_2 \cdot nH_2O$ nanoplates, and HRTEM images (c,d) and SEM images of (e,f) $Zn_3V_2O_7(OH)_2 \cdot nH_2O$ at different magnifications.

(adsorbed or crystal), hydroxyl groups and the phase transformations [2, 13, 15, 25]. A general reaction during the thermal process would likely be as follows:

$$M_3(OH)_2V_2O_7 \cdot nH_2O + \text{heat} \rightarrow M_3V_2O_8 + (n+1)H_2O \quad (M= Co, Ni, Cu, Zn) \quad (3)$$

According to the elimination temperatures listed in Table 1, Co and Ni samples in the amorphous form release crystal waters at lower temperatures compared to Cu and Zn samples when exposed to heat. However, their phase formation temperatures are higher than those of Cu and Zn. By using total weight loss and Equation 3, n values can be deduced as shown in Table 2.

The mol number (2.8) of water found in the $Zn_3(OH)_2V_2O_7 \cdot nH_2O$ and $Co_3(OH)_2V_2O_7 \cdot nH_2O$ compounds was higher than that reported in the literature [4, 24, 26]. This is probably due to the fact that the crystals are arranged in abundant water. However, $Cu_3(OH)_2V_2O_7 \cdot nH_2O$ included only 2 moles of water as in previous reports [7, 14-16], because its crystal lattice and vacancies do not allow more water molecules to penetrate.

FT-IR spectrums of the samples are depicted in the wavelength region of 600-4000 cm^{-1} in Fig. 6. While the spectral shapes of the samples are very similar, the locations and intensities of the peaks are different due to use of different metals. Several intense absorption peaks in 600–950 cm^{-1} region correspond to V–O–M (Co, Ni, Cu, Zn), V-O-V

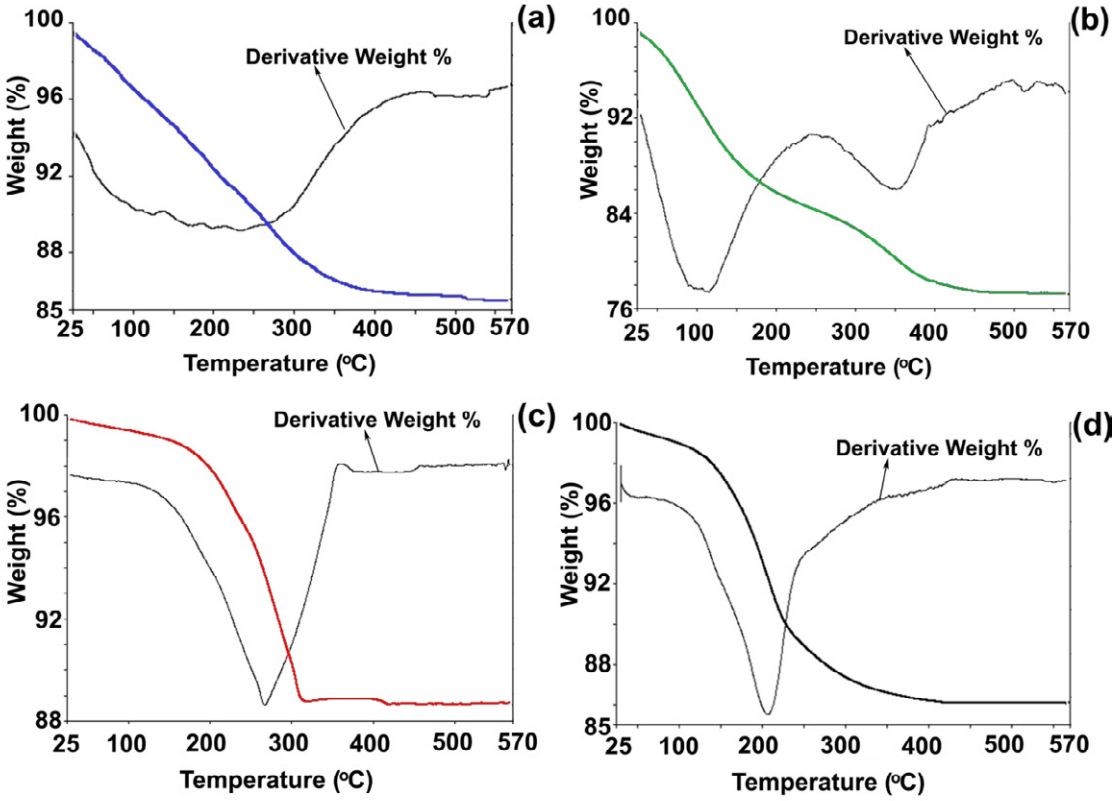

Fig. 5. TGA curves of the as-prepared $Co_3(OH)_2V_2O_7$. nH_2O (a), $Ni_3(OH)_2V_2O_7$. nH_2O (b), $Cu_3(OH)_2V_2O_7$. nH_2O (c) and $Zn_3(OH)_2V_2O_7$. nH_2O (d) compounds.

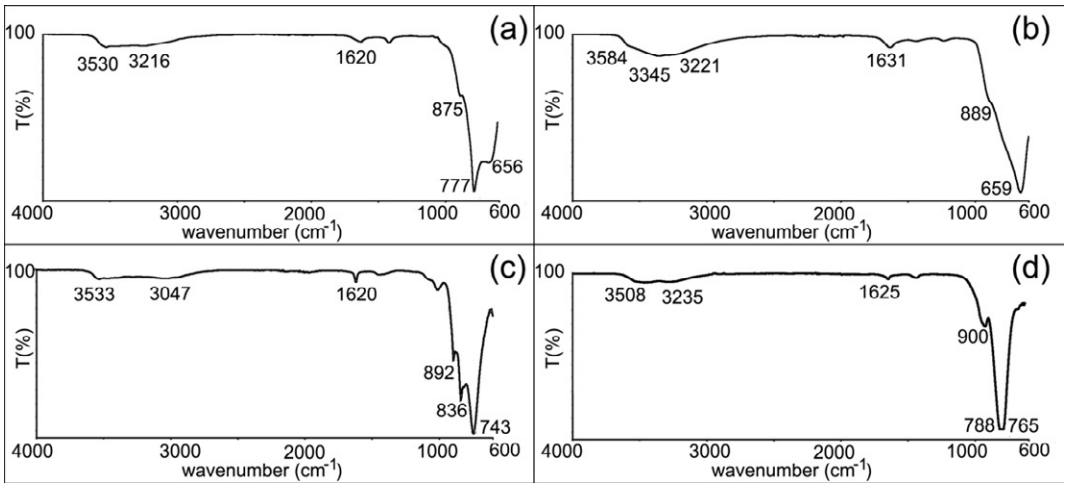

Fig. 6. FT-IR spectrums of the as-prepared $Co_3(OH)_2V_2O_7$. $2.8H_2O$ (a), $Ni_3(OH)_2V_2O_7$. $5.6H_2O$ (b), $Cu_3(OH)_2V_2O_7$. $2H_2O$ (c) and $Zn_3(OH)_2V_2O_7$. $2.8H_2O$ (d) compounds.

symmetric and asymmetric vibrations. Moreover, the peaks around 3500 cm^{-1} and 1620 cm^{-1} are attributed to the symmetric stretching vibration and bending vibration of H–O–H in H_2O molecules, respectively. The other strong and broad peaks around 3200 cm^{-1} belong to the OH group in the framework. The absorption peaks of $Ni_3(OH)_2V_2O_7$. 5.6 H_2O in 3000–3500 cm^{-1} region is stron-

Table 2. Elimination temperatures and total weight losses obtained from TGA.

Metal type	Temperature ranges for elimination of water and hydroxyl (°C)	Temperature ranges for the phase formations (°C)	Total weight loss (%)	n (calculated)
Ni	(58-157) (303-353)	(497-550)	22.80	5.6
Co	(55-268)	(507-518)	14.45	2.8
Cu	(248-312)	(375-460)	11.42	2
Zn	(160-253)	(350-420)	13.86	2.8

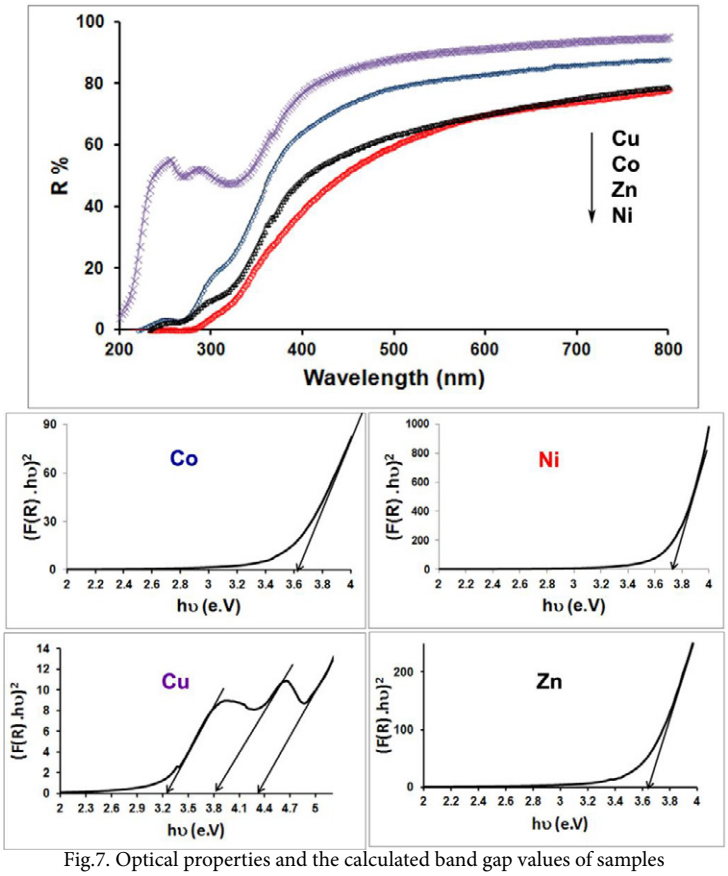

Fig.7. Optical properties and the calculated band gap values of samples

ger than the others because of the presence of more water molecules and amorphous structure. Obviously, all identifying functional groups from IR spectrums are consistent with the previous reports [1, 3, 15, 24].

Fig. 7 shows UV-Vis reflection spectrum which is a useful tool for determining optical band gap in semiconductor materials. At all samples, it displayed a high reflection in the region from 400 to 800 nm. And then, the reflection decreased sharply in the range from 300 to 400 nm. The optical band gap (E_g) was calculated using the following equation: $F(R).h\nu=k\,(h\nu-E_g)^{1/n}$, where hν is the photo energy, k is a constant relative to the material, $F(R)=\frac{(1-R)^2}{2R}$ (R: reflectance) and n is either 2 for direct transition or ½ for indirect transition. The band gaps of the samples were deduced by plotting $(F(R)\cdot h\nu)^2$ vs. hν as shown in Fig. 7. These are 3.62 (Co), 3.77 (Ni), 3.22, 3.80, 4.34 (Cu) and 3.63 (Zn) eV, which are consistent with the literature values [4, 9, 20, 26] .

Effect of concentration at Co and Ni samples

In order to obtain more crystalline nickel hydroxy vanadate nanoparticles, we firstly increased the concentration of reactants by maintaining the other parameters. Then, NaOH concentration was increased from 60 to 100 mmol at 60/20/30 (mmol) of reactant concentration, so, the final pH values measured also increased from 8.27 to 12.5, whereas

Component	Mass (%)
NiO	56.0082
V_2O_5	43.9018
Na_2O	0.0346
SiO_2	0.0554

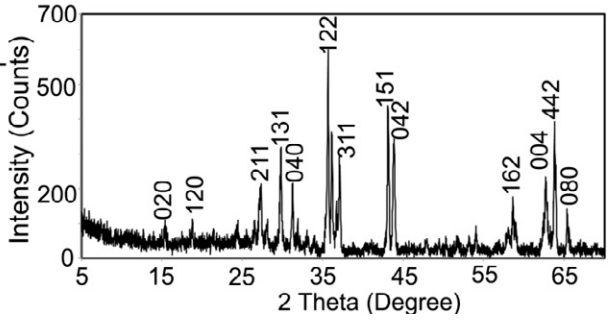

Fig. 8. XRF values of $Ni_3(OH)_2V_2O_7$. nH_2O synthesized by the co-precipitation method and XRD pattern of $Ni_3(OH)_2V_2O_7$. nH_2O annealed at 600 °C for 3 h.

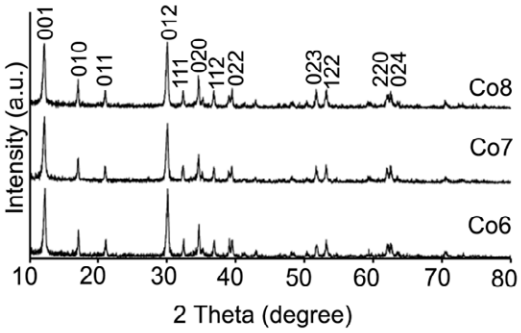

Fig. 9. XRD patterns of samples obtained using 40 mmol (Co6) and 45 mmol (Co7) and 50 mmol (Co8).

for Ni, we could not get a good crystal product at all. Thus, XRF analysis was done for Ni compound with amorphous structure. According to the XRF analysis values in Fig. 8, the Ni/V ratio in the compound is 3/2. Moreover, $Ni_3(OH)_2V_2O_7.nH_2O$ was calcined at 600 °C for 3 hours for testing the crystallite composition of Ni nanoparticles and then the XRD analysis was performed as shown in Fig. 8.

Those diffraction peaks are in accordance with $Ni_3V_2O_8$ which is in agreement with JCPDS, No 74-1485 [27]. Therefore, this structure confirms the thermal procedure at Eq.3, and the estimated compound formulation is found as $Ni_3(OH)_2V_2O_7$ .5.6 H_2O.

In contrast to nickel, good crystalline cobalt hydroxy vanadate nanoparticles would be obtained by increasing the concentration of reactants. The XRD patterns in Fig. 9 show that the peaks of Co6, Co7 and Co8 samples are considerably stronger and sharper than those of Co at Fig. 2 (a), indicating more crystalline phases.

Karpenkoite, $Co_3(OH)_2V_2O_7.nH_2O$, is the cobalt analogue of $Zn_3(OH)_2V_2O_7.nH_2O$ [28] and its synthetic analogue [17]. In particular, the stoichiometry of both minerals is identical (effective ionic radii are 0.74 Å and 0.75 Å for Zn^{2+} and Co^{2+}, respectively) and their crystal morphology and physical properties are very close. Therefore, the diffraction peaks in Fig. 2(a) and Fig. 9 are in accordance with hexagonal phase of $Zn_3(OH)_2V_2O_7.nH_2O$ as also reported previously [26].

The effect of reactant concentrations on the structural properties of cobalt compounds (Co1-Co8) were also investigated by FT-IR, as shown in Fig. 10. As the concentration increased, the OH vibration band (around 3200 cm^{-1}) in the crystal framework became stronger and more prominent, as a result of the increase in crystallinity. Interestingly, other bands growing stronger with increasing crystallinity are 1410 cm^{-1} and 1620 cm^{-1}, attributed to the absorption of NH_4^+ and H_2O molecules on the vanadate compounds, respectively [29, 30]. The $V_2O_7^{4-}$ ion in the $Co_3(OH)_2V_2O_7$. $2.8H_2O$ is composed of two tetrahedral units $(O_3V\text{-}O\text{-}VO_3)^{4-}$ formed by the bridgical use of oxygen. The absorption band at 883 cm^{-1}, corresponding to the symmetric stretching of terminal VO_3 units, shifted to 875 cm^{-1} and became stronger. Moreover, the

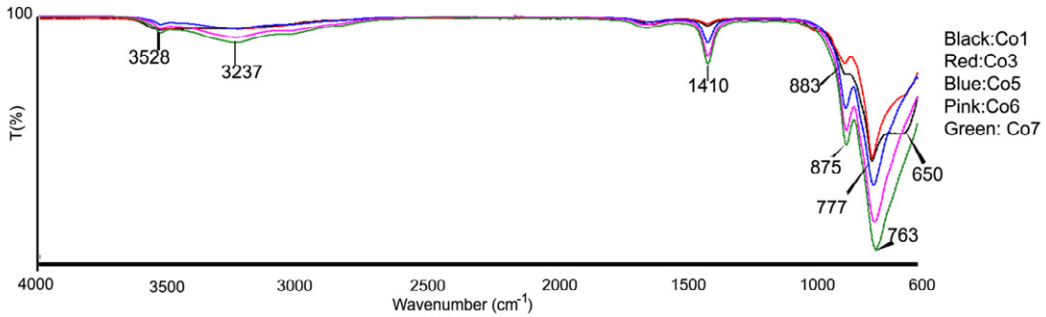

Fig. 10. FT-IR spectrums of the $Co_3(OH)_2V_2O_7.2.8H_2O$ samples synthesized in various concentrations of reactants (Co1, Co3, Co5, Co6, Co7).

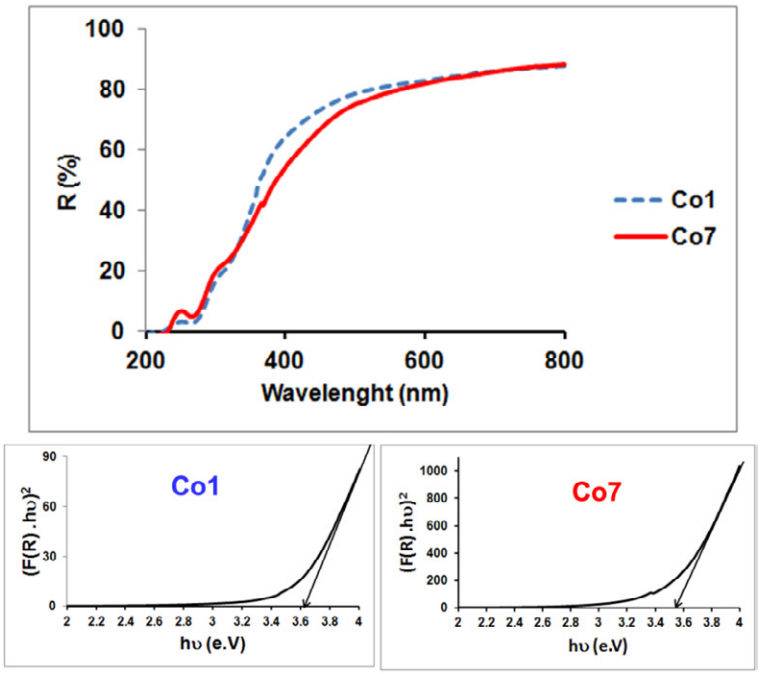

Fig. 11. Effect of concentration on the optical properties of Co samples.

antisymmetric stretching of bridging V-O-V units at 777 cm^{-1} also shifted to 763 cm^{-1} and expanded by overlapping the absorption band (the symmetric stretching of VOV) at 650 cm^{-1} [31]. Thus, as the crystallization increases, the characteristic vibrations become stronger and more pronounced as previously reported [24].

Fig .11 shows UV-visible diffuse reflectance measurements of Co1 and Co7 samples and the graphics of $(F(R) . h\nu)^2$ to hν. The calculated band gaps are 3.61 and 3.57 eV for Co1 and Co7, respectively. According to these results, it can be said that there is no significant effect of the reactant concentration on the optical properties of the Co samples.

Fig. 12a- b shows the *M(H)* curves of Co1, Co4, Co6 and Co8 samples measured in an applied magnetic field range from -5 T and +5 T at 5 K and 300 K temperatures, respectively. The magnetic hysteresis loops indicate ferromagnetic (FM) coupling for the samples at 5 K temperature. From Figs. 12a-b, the reduction in magnetization by increasing Co concentration is due to increasing Co^{2+} clusters with antiferromagnetically coupled moments, in good agreement with earlier reports [32, 33]. In contrast to low temperature experiment, the magnetization response to applied magnetic field becomes linear at room temperature that indicates samples are paramagnetic in nature (Fig. 12b). In

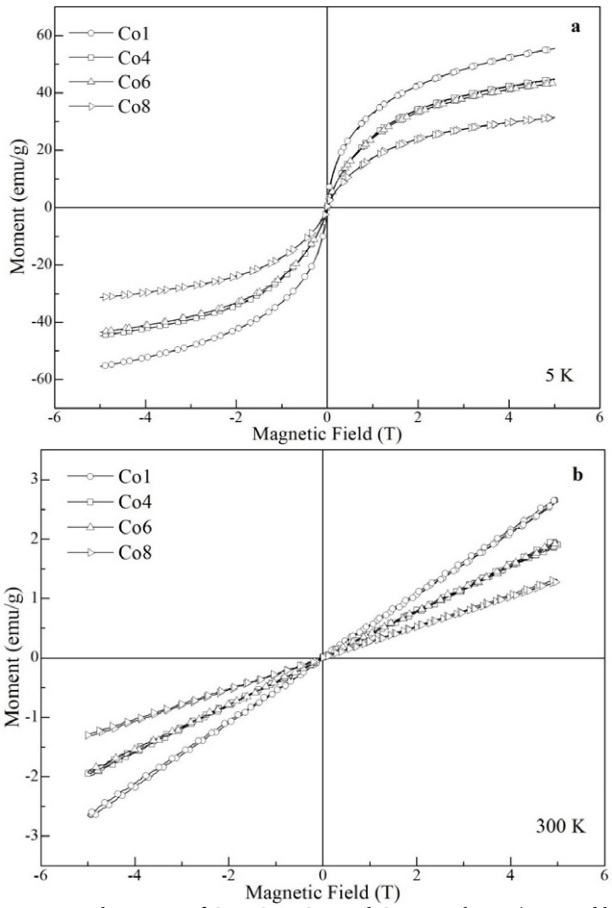

Fig. 12. Magnetic hysteresis of Co1, Co4, Co6 and Co8 samples at a) 5 K and b) 300 K.

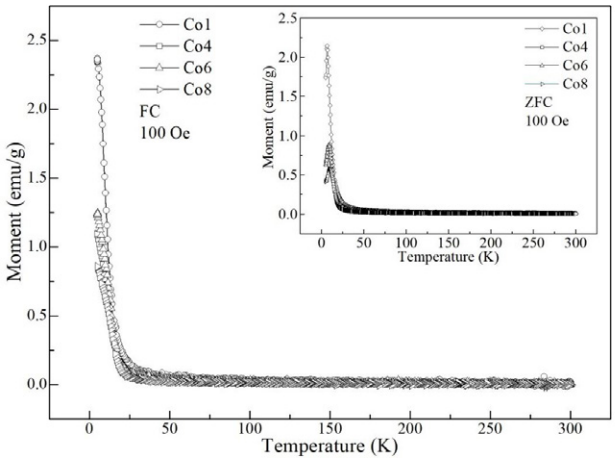

Fig. 13. Field-cooled temperature dependence of magnetization of Co1, Co4, Co6 and Co8 samples under 100 Oe magnetic field. Inset: ZFC curves as a function of temperature.

addition to field dependence of magnetization experiments, we performed temperature dependence of magnetization, *M(T)* measurements by sweeping temperature from 2 to 300 K for field-cooled (FC) and zero-field-cooled (ZFC) conditions under 100 Oe external magnetic field (Fig. 13). The ZFC and FC curves of samples nearly follow the same path that the magnetization first decreases sharply with

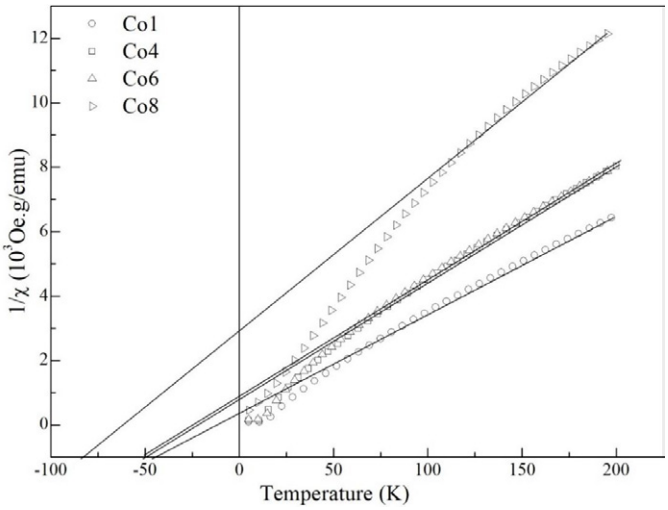

Fig. 14. Inverse DC-magnetic susceptibility curves as a function of temperature of Co1, Co4, Co6 and Co8 samples.

increasing temperature (2-25 K) and stays almost zero magnetization even after further temperature (25-300 K). This region of curves is assigned to a typical paramagnetic behavior.

In order to compare the magnetic coupling degree of Co1, Co4, Co6 and Co8 samples, we plot the inverse susceptibility $1/\chi$ as a function of T as shown in Fig. 14. The Curie-Weiss law can be applied to this Fig. in the temperature range of 25 to 200 K because the data in this part could be fitted to a straight line. These straight lines cut the temperature axis corresponding to Curie-Weiss temperature, θ. Since the sign and magnitude of θ are related to the strength of coupling between magnetic ions in the lattice [34, 35], we first determined the Curie-Weiss temperature using the following relation;

$$\frac{1}{\chi} = \frac{T-\theta}{C}$$

where C is the Curie constant. The θ values obtained from the Fig. 14 are -44.20, -48.74, -49.65 and -82.37 for Co1, Co4, Co6 and Co8 samples, respectively. Negative θ values indicate that the samples have antiferromagnetic interaction [36]. It is interesting to point out that the magnitude of θ values increase with increasing Co concentration. It means that Co8 sample has a stronger antiferromagnetic interaction than Co1. Further magnetic analysis has been performed by the effective magnetic moment of the samples calculated using the following relation:

$$\mu_{eff} = \sqrt{3k_B CM/N_A}$$

where N_A, M and k_B are the Avogadro number, molecular weights of the samples and Boltzmann constant, respectively. The effective magnetic moment of Co1, Co4, Co6 and Co8 samples are found to be 3.75, 3.42, 3.40 and 2.72μ_B, respectively. The trend of effective magnetic moment as a function of Co amount is consisted with the results of hysteresis measurements.

CONCLUSION

We demonstrated that the recently new approach proposed for the preparation of $LnVO_4$ nanoparticles at room temperature is also successful for the preparation of $M_3(OH)_2V_2O_7{\cdot}nH_2O$ (M : Co, Ni, Cu, Zn) nanostructures. Reaction conditions were mild and reaction process was simple and feasible, offering great opportunities for the scale-up preparation of metal vanadates with different morphologies. This study also shows how the metal type can affect the properties of the final products. For example, $Ni_3(OH)_2V_2O_7.nH_2O$ is always amorphous and includes very small (9 nm) nanoparticles with irregular shape. $Co_3(OH)_2V_2O_7.nH_2O$ nanoparticles also are very small and not good crystalline but it is possible to obtain better crystals by increasing the reactant concentrations. The best crystalline phase was observed for zinc and copper compounds. These results revealed a relation between the crystallinity and the tendency of these metals to complex with the NH_3 molecules,

for the first time. The shapes of $Cu_3V_2O_7(OH)_2 \cdot nH_2O$ and $Zn_3V_2O_7(OH)_2 \cdot nH_2O$ are nanoflake or nanoplate and both have an average diameter of less than 500 nm. Mol numbers of water calculating from TGA curves also changed depending on metal type. The compound formulas were found to be $Co_3(OH)_2V_2O_7.2.8H_2O$, $Ni_3(OH)_2V_2O_7$. $5.6H_2O$, $Cu_3(OH)_2V_2O_7.2H_2O$ and $Zn_3(OH)_2V_2O_7.2.8H_2O$. In the magnetic experiments, all Co samples show similar trend in both temperature and external field dependence magnetizations. Verified by the Curie-Weiss law, the magnetic coupling is getting weaker when Co amount increased in the structure..

ACKNOWLEDGEMENTS

This work was supported by Balikesir University Research Project, Grant no. BAP 2015/60.

CONFLICT OF INTEREST

The author declared to no conflict of interest.

REFERENCES

1. Ni S, He D, Yang X, Li T. ChemInform Abstract: Hydrothermal Synthesis of Cu3 (OH)2V2O7·nH2O Nanoparticles and Its Application in Lithium Ion Battery. ChemInform. 2011;42(13):no-no.
2. Ni S, Zhou G, Lin S, Wang X, Pan Q, Yang F, et al. Hydrothermal synthesis of Zn3(OH)2V2O7·nH2O nanosheets and its application in lithium ion battery. Materials Letters. 2009;63(28):2459-61.
3. Ren M, Song J, Shi Y, Xiang Y, Hu G. Synthesis of zinc pyrovanadate 3D flower-like microspheres and their photocatalytic properties. Journal of Crystal Growth. 2014;402:119-23.
4. Wang F, Wu W, Sun X, Song S, Xing Y, Wang J, et al. Synthesis of hexagonal Zn3(OH)2V2O7·2H2O nanoplates by a hydrothermal approach: Magnetic and photocatalytic properties. Materials Characterization. 2013;86:139-45.
5. Hu Y-Y, Liu Z, Nam K-W, Borkiewicz OJ, Cheng J, Hua X, et al. Origin of additional capacities in metal oxide lithium-ion battery electrodes. Nature Materials. 2013;12(12):1130-6.
6. Nam KW, Kim S, Lee S, Salama M, Shterenberg I, Gofer Y, et al. The High Performance of Crystal Water Containing Manganese Birnessite Cathodes for Magnesium Batteries. Nano Letters. 2015;15(6):4071-9.
7. Zhang S, Ci L, Liu H. Synthesis, Characterization, and Electrochemical Properties of Cu3V2O7(OH)2·2H2O Nanostructures. The Journal of Physical Chemistry C. 2009;113(20):8624-9.
8. Liu P, Liang Y, Lin X, Wang C, Yang G. A General Strategy To Fabricate Simple Polyoxometalate Nanostructures: Electrochemistry-Assisted Laser Ablation in Liquid. ACS Nano. 2011;5(6):4748-55.
9. Liang Y, Liu P, Li HB, Yang GW. Synthesis and characterization of copper vanadate nanostructures via electrochemistry assisted laser ablation in liquid and the optical multi-absorptions performance. CrystEngComm. 2012;14(9):3291.
10. Bulbul B, Beyaz S. Strong paramagnetic crystalline LnVO4 (Ln: Gd, Tb, Dy, Ho, Er) nanoparticles synthesized by a fabricating method. Materials Chemistry and Physics. 2016;173:200-4.
11. Bulbul B, Beyaz S. An effective synthesis of crystalline Pb 5 (VO 4) 3 OH nanorods. Nano-Structures & Nano-Objects. 2017;10:100-4.
12. Lafontaine MA, Le Bail A, Férey G. Copper-containing minerals—I.Cu3V2O7(OH)2,2H2O:Thesynthetichomolog of volborthite; crystal structure determination from X-ray and neutron data; structural correlations. Journal of Solid State Chemistry. 1990;85(2):220-7.
13. Ni S, Wang X, Zhou G, Yang F, Wang J, He D. Hydrothermal synthesis and magnetic property of Cu3(OH)2V2O7·nH2O. Materials Letters. 2010;64(4):516-9.
14. Zhang SY, Ci LJ. Synthesis and formation mechanism of Cu3V2O7(OH)2·2H2O nanowires. Materials Research Bulletin. 2009;44(10):2027-32.
15. Melghit K, Yahaya AH, Yaacob II. Room temperature synthesis of copper pyrovanadate; the effect of stirring time. Materials Letters. 2003;57(8):1423-7.
16. Ghiyasiyan-Arani M, Masjedi-Arani M, Ghanbari D, Bagheri S, Salavati-Niasari M. Novel chemical synthesis and characterization of copper pyrovanadate nanoparticles and its influence on the flame retardancy of polymeric nanocomposites. Scientific Reports. 2016;6(1).
17. Zavalij PY, Zhang F, Whittingham MS. A New Zinc Pyrovanadate, Zn3(OH)2V2O7.2H2O, from X-ray Powder Data. Acta Crystallographica Section C Crystal Structure Communications. 1997;53(12):1738-9.
18. Zavalij PY, Zhang F, Whittingham MS. The zinc–vanadium–oxygen–water system: hydrothermal synthesis and characterization. Solid State Sciences. 2002;4(5):591-7.
19. Wang Q, Zheng L, Bai Y, Zhao J, Wang F, Zhang R, et al. Zn3(OH)2V2O7·2H2O/g-C3N4: A novel composite for efficient photodegradation of methylene blue under visible-light irradiation. Applied Surface Science. 2015;347:602-9.
20. Shi R, Wang Y, Zhou F, Zhu Y. Zn3V2O7(OH)2(H2O)2 and Zn3V2O8 nanostructures: controlled fabrication and photocatalytic performance. Journal of Materials Chemistry. 2011;21(17):6313.
21. Ni S, Lin S, Pan Q, Huang K, Yang F, He D. Crystallized Zn3(OH)2V2O7·nH2O: Hydrothermal synthesis and magnetic property. Journal of Alloys and Compounds. 2009;477(1-2):L1-L3.
22. Ni S, Wang X, Sun X, Yang F, Liu Y, He D. Optical properties of Zn3(OH)2V2O7·nH2O nanosheets. Materials Chemistry and Physics. 2010;124(1):803-8.
23. Ni S, Zhou G, Wang X, Sun X, Yang F, Liu Y, et al. Synthesis of Zn3(OH)2V2O7·nH2O hierarchical nanostructures and their photoluminescence properties. Materials Chemistry and Physics. 2010;120(2-3):426-30.
24. Melghit K, Al-Belushi AK, Al-Amri I. Short reaction time preparation of zinc pyrovanadate at normal pressure. Ceramics International. 2007;33(2):285-8.
25. Wang M, Shi Y, Jiang G. 3D hierarchical Zn3(OH)2V2O7·2H2O and Zn3(VO4)2 microspheres: Synthesis, characterization and photoluminescence. Materials Research Bulletin. 2012;47(1):18-23.
26. Ni S, Li T, Yang X. Synthesis of Co3(OH)2V2O7·1.7H2O nanosheets and its application in lithium ion batteries.

Materials Letters. 2011;65(17-18):2662-4.
27. Kumarasiri A, Lawes G. Control of the multiferroic transition in Ni3V2O8by transition metal doping. Physical Review B. 2011;84(6).
28. Kasatkin AV, Plášil J, Pekov IJ, Belakovskiy DI, Nestola F, Čejka J, et al. Karpenkoite, Co3(V2O7)(OH)2·2H2O, a cobalt analogue of martyite from the Little Eva mine, Grand County, Utah, USA. Journal of Geosciences. 2015:251-7.
[29] Weiss P, Lapkowski M, Legeros R, Bouler J-M, Jean A, Daculsi G. FTIR spectroscopic study of an organic/mineral composite for bone and dental substitute materials. J Mater Sci Mater Med. 1997;8(10):621.
30. Rossetti I, Mancini GF, Ghigna P, Scavini M, Piumetti M, Bonelli B, et al. Spectroscopic Enlightening of the Local Structure Of VOX Active Sites in Catalysts for the Odh of Propane. The Journal of Physical Chemistry C. 2012;116(42):22386-98.
31. Frost RL, Erickson KL, Weier ML, Carmody O. Raman and infrared spectroscopy of selected vanadates. Spectrochimica Acta Part A: Molecular and Biomolecular Spectroscopy. 2005;61(5):829-34.
32. Risbud AS, Spaldin NA, Chen ZQ, Stemmer S, Seshadri R. Magnetism in polycrystalline cobalt-substituted zinc oxide. Physical Review B. 2003;68(20).
33. Lawes G, Risbud AS, Ramirez AP, Seshadri R. Absence of ferromagnetism in Co and Mn substituted polycrystalline ZnO. Physical Review B. 2005;71(4).
34. Chen W, Zhao LF, Wang YQ, Miao JH, Liu S, Xia ZC, et al. Magnetism in Mn-doped ZnO bulk samples. Solid State Communications. 2005;134(12):827-30.
35. Akyol M, Ekicibil A, Kiymaç K. DC Magnetic Properties of the Ho doped ZnO Compounds. Journal of Superconductivity and Novel Magnetism. 2013;26(11):3257-62.
36. Akyol M, Ekicibil A, Kiymaç K. AC-magnetic susceptibility of Dy doped ZnO compounds. Journal of Magnetism and Magnetic Materials. 2015;385:65-9.